Monthly Notices
of the
ROYAL ASTRONOMICAL SOCIETY

MNRAS **475,** 257–265 (2018)
Advance Access publication 2017 December 13

doi:10.1093/mnras/stx3217

AGB subpopulations in the nearby globular cluster NGC 6397

B. T. MacLean,[1★] S. W. Campbell,[1,2] G. M. De Silva,[3,4] J. Lattanzio,[1] V. D'Orazi,[5,6,7] P. L. Cottrell,[1,8] Y. Momany[7] and L. Casagrande[9]

[1]*Monash Centre for Astrophysics, School of Physics and Astronomy, Monash University, Victoria 3800, Australia*
[2]*Max-Planck-Institut für Astrophysik (MPA), Karl-Schwarzschild-Strasse 1, D-85748 Garching, Germany*
[3]*Australian Astronomical Observatory, 105 Delhi Rd, North Ryde, NSW 2113, Australia*
[4]*Sydney Institute for Astronomy, School of Physics, The University of Sydney, NSW 2006, Australia*
[5]*Research Centre for Astronomy, Astrophysics & Astrophotonics (MQAAAstro), Macquarie University, Sydney, NSW 2109, Australia*
[6]*Department of Physics and Astronomy, Macquarie University, North Ryde, NSW 2109, Australia*
[7]*INAF Osservatorio Astronomico di Padova, vicolo dell'Osservatorio 5, I-35122 Padova, Italy*
[8]*School of Physical and Chemical Sciences, University of Canterbury, Private Bag 4800, Christchurch 8140, New Zealand*
[9]*Research School of Astronomy and Astrophysics, Australian National University, Canberra, ACT 2611, Australia*

Accepted 2017 December 7. Received 2017 November 16; in original form 2017 May 21

ABSTRACT

It has been well established that Galactic Globular clusters (GCs) harbour more than one stellar population, distinguishable by the anticorrelations of light-element abundances (C–N, Na–O, and Mg–Al). These studies have been extended recently to the asymptotic giant branch (AGB). Here, we investigate the AGB of NGC 6397 for the first time. We have performed an abundance analysis of high-resolution spectra of 47 red giant branch (RGB) and eight AGB stars, deriving Fe, Na, O, Mg, and Al abundances. We find that NGC 6397 shows no evidence of a deficit in Na-rich AGB stars, as reported for some other GCs – the subpopulation ratios of the AGB and RGB in NGC 6397 are identical, within uncertainties. This agrees with expectations from stellar theory. This GC acts as a control for our earlier work on the AGB of M4 (with contrasting results), since the same tools and methods were used.

Key words: stars: abundances – stars: AGB and post-AGB – Galaxy: abundances – Galaxy: formation – globular clusters: general.

1 INTRODUCTION

It is well known that Galactic globular clusters (GCs) show star-to-star spreads in the abundances of proton-capture elements (primarily He, C, N, O, and Na), while most GCs remain homogeneous in the iron peak species (Carretta et al. 2009b). This spread often presents as multimodal [as in the early low-resolution cyanogen (CN) studies of Cottrell & Da Costa (1981) and Norris (1981)], with two or more distinct subpopulations being identified. One of these subpopulations is always chemically similar to Galactic halo stars of the same metallicity – designated here as SP1 and which is inferred to contain primordial He abundances – with one or more further subpopulations found to have higher N and Na (and lower C and O) abundances – here designated collectively as SP2 (see Gratton, Carretta & Bragaglia 2012, for an extensive review). These are the ubiquitous C–N and Na–O (and Mg–Al in some GCs) anticorrelations (Carretta et al. 2009a). This spread in light-elemental abundance can also be inferred from narrow and intermediate band photometric data, seen as multiple red- or sub-giant branches, or multiple main sequences in a GC's colour–magnitude diagram (e.g. Milone et al. 2008, 2014).

The peculiar abundance signature of SP2 stars has been observed in both evolved and unevolved stars in many clusters (Gratton et al. 2001), indicating that this pattern is likely to have been inherited at birth. Furthermore, the pattern is generally not observed elsewhere, such as the (less massive) open clusters of the Galaxy (De Silva et al. 2009; MacLean, De Silva & Lattanzio 2015); however, very recently it has been suggested that the Galactic bulge may contain SP2-like stars (Schiavon et al. 2017). The most common explanation for this light-elemental inhomogeneity is the self-pollution hypothesis where the ejecta of more massive SP1 stars are mixed with an early dense interstellar medium, from which SP2 stars were formed (Cannon et al. 1998; Gratton, Sneden & Carretta 2004).

Importantly, the relative fractions of each subpopulation remain the same through all these phases of evolution, as expected from stellar evolutionary theory. However, until recently there were no systematic surveys of asymptotic giant branch (AGB) stars. Some early (e.g. Norris et al. 1981) and more recent (Campbell et al. 2010, 2013) low-resolution spectroscopic studies of GCs found that the distribution of CN band strengths varies greatly between the red giant branch (RGB) and AGB of several GCs. In particular, they

★ E-mail: ben.maclean@monash.edu

found no CN-strong (i.e. SP2) AGB stars in NGC 6752, which has an extended blue horizontal branch (HB). These results hinted at differences in evolution between stars of different light-elemental abundances, which are not fully predicted in standard stellar evolution theory – only stars with extreme He abundances are expected to avoid the AGB phase due to smaller envelopes in the HB phase (Dorman, Rood & O'Connell 1993; Campbell et al. 2013; Cassisi et al. 2014).

In this paper, we use the prescription as described in MacLean et al. (2016, hereafter ML16), where the percentages of RGB and AGB stars in a GC that are found to be members of SP2 are written as $\mathscr{R}_{\rm RGB}$ and $\mathscr{R}_{\rm AGB}$, respectively (typical $\mathscr{R}_{\rm RGB}$ values are ∼50–70 per cent; Carretta et al. 2010); and the SP2 AGB deficit is given by

$$\mathscr{F} = \left(1 - \frac{\mathscr{R}_{\rm AGB}}{\mathscr{R}_{\rm RGB}}\right) \cdot 100 \text{ per cent}, \quad (1)$$

where a value of 100 per cent indicates that no SP2 stars reach the AGB – as reported for NGC 6752 and M62 by Campbell et al. (2013) and Lapenna et al. (2015), respectively. For clusters with extended HBs (where the bluest stars reach $T_{\rm eff}$ over 15 000 K; e.g. NGC 6752, NGC 2808), an $\mathscr{F}$ value of up to ∼30 per cent may be expected due to the well-established existence of AGB-manqué stars (which evolve directly from the HB to the white dwarf phase, avoiding the AGB; Greggio & Renzini 1990; Dorman et al. 1993; Cassisi et al. 2014). Clusters whose HBs do not extend into this regime (e.g. M4, NGC 6397) are expected to have an $\mathscr{F}$ value of zero per cent, with all stars in the cluster ascending the AGB.

There has been much debate as to the level and existence of GC SP2 AGB deficits in recent years as more evidence has been gathered, but a definitive conclusion has yet to be reached. In fact, contradictory evidence has been presented for both NGC 6752 and M4. For example, in Campbell et al. (2013), we found that the measured Na abundances in all NGC 6752 AGB stars were consistent with SP1, indicating $\mathscr{F} \sim 100$ per cent. Lapenna et al. (2016) conducted an independent study of the same GC, and found that with [Na I/Fe I] abundances, $\mathscr{F}$ dropped to the predicted value of ∼30 per cent. The assumption that dividing by Fe I is more accurate has recently been disputed by Campbell et al. (2017, hereafter C17). Recent studies of AGB stars in other GCs such as Johnson et al. (2015), García-Hernández et al. (2015), and Wang et al. (2016) have found varying values of $\mathscr{F}$ – see table 4 of ML16 for a summary of $\mathscr{F}$ values as of 2016 July.

Attempts to theoretically explain SP2 AGB deficits have been outpaced by the numerous observational studies that have painted a complex picture, both technically (e.g. the treatment of non-local thermodynamic equilibrium – LTE) and empirically (e.g. contradictory results). If high SP2 AGB deficits are real, rather than being an artefact of the spectroscopic analysis (see Section 5 for discussion), then the most likely explanation comes from the He-enrichment of SP2 stars. This results in smaller envelope masses on the HB (Gratton et al. 2010; Cassisi et al. 2014; Charbonnel & Chantereau 2016) and such stars are known to evolve directly to the white dwarf phase (AGB-manqué stars). SP2 AGB deficits above $\mathscr{F} \simeq 30$ per cent suggest that the location along the HB where this alternative evolutionary path begins to occur may be incorrectly predicted by theory, and/or dependent on more factors than previously thought.

Similar to the debate on AGB abundances in NGC 6752, recent studies on the archetypal GC M4 have presented starkly different conclusions on the nature of its AGB. ML16 presented [Na/Fe] and [O/Fe] abundances for both AGB and RGB stars in M4, reaching the conclusion that all AGB stars are consistent with being SP1 stars (i.e. $\mathscr{F} \simeq 100$ per cent). In contrast, Lardo et al. (2017) and Marino et al. (2017), using photometric indices and spectroscopic analysis, respectively, concluded that the spread of light-elemental abundances in the AGB of M4 is similar to the RGB (however, both studies found that their AGB samples were offset towards SP1-like abundances). If true, this is consistent with the theoretical prediction of $\mathscr{F} = 0$ per cent. However, the very recent study of Wang et al. (2017) showed that the spread in Na abundances of M4's AGB is significantly narrower than the RGB, qualitatively similar to the findings of ML16, but not as extreme. It is clear that further study of this GC is required.

If high SP2 AGB deficits are reliably demonstrated, this may impose new and important restrictions on low-mass, low-metallicity stellar evolution and/or atmospheric models; impacting the field of globular clusters, stellar evolution, and Galactic formation and archaeology.

In the current study, we aim to derive AGB subpopulation ratios for the GC NGC 6397 for the first time. NGC 6397 is an old and metal-poor GC with a well-documented Na–O anticorrelation on the RGB, the range of which is smaller than many other clusters (no 'extreme population' in the classification of Carretta et al. 2009b, which is associated with high He abundance). NGC 6397 also displays an Mg–Al anticorrelation (Lind et al. 2011a, hereafter L11). The short (but blue) HB of NGC 6397 extends between $8000\,{\rm K} < T_{\rm eff} < 10\,500\,{\rm K}$, suggesting that no stars in the cluster should evolve into AGB-manqué stars (Lovisi et al. 2012). In order to determine if this is the case, we have performed an analysis of spectra from a sample of AGB and RGB stars in NGC 6397. For each star, we have derived radial velocities, stellar parameters, and abundances of Fe, Na, O, Mg, and Al.

2 SAMPLE SELECTION, OBSERVATIONS, AND MEMBERSHIP

Our stellar targets were selected from the NGC 6397 photometric data set of Momany et al. (2003, UBVI from the ESO/MPG WFI, see Table 1). For the bright stars considered here, the photometric completeness is 100 per cent for all colours. The photometry covers the entire cluster out to at least 9 arcmin from the cluster centre (in some directions reaching to ∼22 arcmin). This compares with the cluster's half-light radius of 2.9 arcmin (Harris 1996). To avoid crowding problems in the core with multi-object fibre placement, the sample was limited to stars outside ∼0.5 arcmin of the cluster centre.

The RGB and AGB are separated in $V-(B-V)$ and $U-(U-I)$ space (Fig. 1). AGB stars were conservatively selected – only early-AGB stars were included so as to avoid the mislabelling of stars since the AGB and RGB colours become similar at brighter magnitudes. We then cross-matched our selection with the 2MASS data base to take advantage of the high-quality astrometry and JHK photometry. 2MASS IDs and JHK photometric magnitudes for the whole sample are included in Table 1. In total, our initial target sample included nine AGB stars and 64 RGB stars. Importantly for the science goal of this study, the RGB and AGB samples are spatially coincident.

High-resolution spectra were collected in 2015 July using 2dF+HERMES on the Anglo-Australian Telescope which provides $R = 28\,000$ spectra in four narrow windows; blue (4715–4900 Å), green (5649–5873 Å), red (6478–6737 Å), and infrared (7585–7887 Å) (for more details on the HERMES instrument, see De Silva et al. 2015; Sheinis et al. 2015). Due to restrictions on 2dF fibre positioning, we were able to collect spectra for only 60 of the

Table 1. NGC 6397 target details including data from Momany et al. (2003, UBVI photometry and target IDs) and 2MASS (Skrutskie et al. 2006, *JHK* photometry – gaps in data represent targets with low-quality flags), radial velocities (km s^{-1}), and L11 IDs. Full table available online.

ID	Type	2MASS ID	L11 ID	*V* Mag	*B* Mag	*U* Mag	*I* Mag	*J* Mag	*H* Mag	*K* Mag	RV (km s^{-1})
56897	AGB	17400665-5335001	–	11.83	12.76	10.59	13.11	9.76	9.25	9.13	17.17
60609	AGB	17402547-5347570	–	11.65	12.62	10.37	12.97	–	–	–	20.68
70509	AGB	17405254-5341049	–	11.98	12.90	10.75	13.17	9.95	9.48	9.31	19.38
70522	AGB	17404076-5341046	–	11.16	12.24	9.79	12.80	8.94	8.37	8.26	18.93
73216	AGB	17403510-5339572	–	11.83	12.76	10.57	13.11	–	–	–	16.00
⋮	⋮	⋮	⋮	⋮	⋮	⋮	⋮	⋮	⋮	⋮	⋮

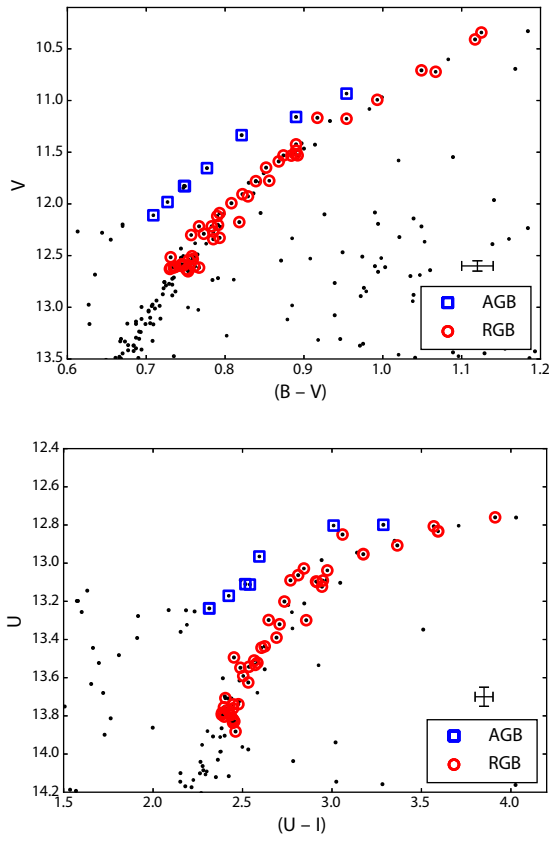

Figure 1. $V-(B-V)$ and $U-(U-I)$ colour–magnitude diagrams of the observed NGC 6397 RGB and AGB stars (open circles and squares, respectively), displayed over the full photometric sample of Momany et al. (2003, black points). In the top panel, a constant reddening correction value of $(B-V)=-0.19$ was applied to all photometric data. No reddening correction was applied to the $(U-I)$ photometry (bottom panel). We note that there are only seven AGB stars in the $U-(U-I)$ diagram because one star (AGB 80621) does not have a reliable *U*-band magnitude and was selected based only on its *B*- and *V*-band magnitudes.

73 targets. This down-sampling is random, except that priority was given to obtaining the largest possible sample of AGB stars, since the number of AGB stars is inherently low compared to RGB stars (see Fig. 1, black dots). In total, we collected spectra for eight of the nine identified AGB stars, and 52 RGB stars.

The spectra had an average signal-to-noise ratio of 70. The software package 2DFDR (AAO Software Team 2015, v6.5) was used to reduce the data for analysis. Radial velocities were measured with the IRAF FXCOR package (Tody 1986), using a solar reference template. The mean radial velocity for NGC 6397 after non-member elimination was found to be $<v> = 19.30 \pm 0.48$ km s^{-1} ($\sigma = 3.71$ km s^{-1}), consistent with Lind et al. (2009), who report $<v> = 18.59 \pm 0.16$ km s^{-1} ($\sigma = 3.61$ km s^{-1}). Individual stellar radial velocities are listed in Table 1. Iterative 3σ clipping of radial velocities and metallicities (discussed in Section 3.2) reduced the final RGB sample to 47 stars. All of the eight observed AGB stars were found to be members.

Apart from not sampling the inner core of the cluster, we do not identify any sample bias. Moreover, we have collected spectra for almost all of the AGB stars in the very wide field of view of the source photometry. The 47 RGB stars offer a solid basis for a comparison. The final observed samples can be seen visually in the colour–magnitude diagrams of Fig. 1, overplotted against the full photometry sample.

3 METHOD

3.1 Atmospheric parameters

For this study, we have used several photometric relations to determine effective temperatures for all stars.

Typically with spectroscopic studies (such as ML16), stellar parameters are determined by requiring the excitation and ionization balance of abundances from neutral and singly ionized iron (Fe I and Fe II, respectively) absorption lines (e.g. Sousa 2014). While a significant strength of this method is that the parameters are unaffected by photometric reddening, there are also many weaknesses. Many solutions can be found for a single star, largely depending on the choice of initial parameter estimates (see C17). Additional spectroscopic uncertainties such as equivalent width (EW) measurements, choice of atmospheric model, atomic line data, and parameter interdependence can compound this problem.

To further complicate the picture, Lapenna et al. (2014, 2016) have provided evidence that the Fe I lines of AGB stars may experience a higher degree of non-LTE effects than RGB stars at the same metallicity and effective temperature. If true, then assuming ionization balance may artificially and preferentially lower the derived surface gravity of AGB stars (Lind, Bergemann & Asplund 2012). In C17, we suggested that this so-called 'AGB iron overionization problem' does not exist (at least in NGC 6752), but may be the result of systematic offsets in photometrically derived $T_{\rm eff}$. Regardless, Fe I lines are well known to experience some non-LTE effects (on both the RGB and AGB, and especially at low metallicities; see Bergemann et al. 2012), so forcing ionization balance prior to the correction of non-LTE effects may result in systematically incorrect gravities and metallicities in all stars.

We have used the $B-V$ and $V-K$ relations from Ramírez & Meléndez (2005), González Hernández & Bonifacio (2009), and Casagrande et al. (2010) to determine $T_{\rm eff}$ estimates. Additionally, we have calculated $T_{\rm eff}$ without relying on colour calibrations, by

Table 2. Average differences in $T_{\rm eff}$ between the adopted value and each photometric estimate. Uncertainties are the 1σ standard deviations of the cluster samples. The average σ value in the last row is indicative of the spread of $T_{\rm eff}$ estimates for each star.

Method	$\Delta T_{\rm eff}$ (K)
Ram $(B-V)^a$	94 ± 45
Gonz $(B-V)^b$	-17 ± 42
Casa $(B-V)^c$	22 ± 98
Ram $(V-K)^a$	69 ± 35
Gonz $(V-K)^b$	-34 ± 34
Casa $(V-K)^c$	-33 ± 32
IRFM	-108 ± 47
Average σ	± 48

Notes. [a]Ramírez & Meléndez (2005)
[b]González Hernández & Bonifacio (2009)
[c]Casagrande et al. (2010)

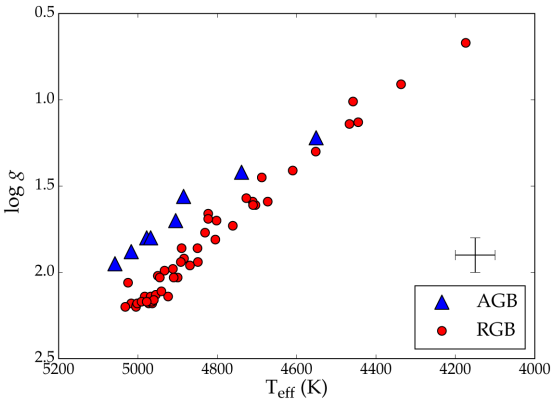

Figure 2. Final stellar parameters of NGC 6397, determined from photometric relations. The method of parameter determination is described in the text. Typical uncertainties are indicated, and are the same as in Table 6.

implementing the infrared flux method (IRFM) at an estimated log g of each AGB and RGB star, as described in Casagrande et al. (2010, 2014) using *BVI* and 2MASS *JHK* photometry. Thus, we have seven $T_{\rm eff}$ estimates for each star. These methods are dependent on metallicity, for which a value of [Fe/H] $= -2.00$ was assumed for NGC 6397. To account for interstellar extinction, we applied a constant correction of $E(B-V) = -0.19$ to all stars (Gratton et al. 2003). NGC 6397 does not suffer from significant differential reddening (Milone et al. 2012).

Four stars were flagged for low quality and/or contamination in the 2MASS data base, so only the $B-V$ relations were used to determine $T_{\rm eff}$ for these stars. For all other stars, the mean of the seven $T_{\rm eff}$ estimates was adopted. Table 2 shows the variation between the final adopted $T_{\rm eff}$ values and those of the photometric relations and IRFM. Surface gravities (log g) and microturbulences ($v_{\rm t}$) were determined using the empirical relations from Alonso, Arribas & Martínez-Roger (1999) and Gratton, Carretta & Castelli (1996), respectively, and assuming a mass of 0.8 and 0.7 $M_\odot$ for the RGB and AGB, respectively (Lovisi et al. 2012; Miglio et al. 2016). We adopt a 1σ uncertainty of ± 50 K for $T_{\rm eff}$ (see Table 2), ± 0.1 dex for log g, and ± 0.2 km s^{-1} for $v_{\rm t}$. Final stellar parameters for each star are included in Table 5 and represented visually in Fig. 2.

Table 3. Adopted line list used for EW measurements. Based on the line list of the GALAH collaboration (De Silva et al. 2015).

Wavelength (Å)	Species	Excitation potential (eV)	log gf
7771.94	O I	9.146	0.369
7774.16	O I	9.146	0.223
7775.39	O I	9.146	0.002
5682.63	Na I	2.100	−0.706
5688.20	Na I	2.100	−0.404
4730.03	Mg I	4.350	−2.347
5711.09	Mg I	4.350	−1.724
7691.53	Mg I	5.750	−0.783
6696.02	Al I	3.140	−1.569
6698.67	Al I	3.140	−1.870
7835.31	Al I	4.020	−0.689
7836.13	Al I	4.020	−0.534
4788.76	Fe I	3.237	−1.763
4839.54	Fe I	3.270	−1.820
4890.75	Fe I	2.875	−0.394
4891.49	Fe I	2.849	−0.111
5701.56	Fe I	2.559	−2.220
5753.12	Fe I	4.260	−0.690
5859.59	Fe I	4.549	−0.419
5862.36	Fe I	4.549	−0.127
6498.94	Fe I	0.958	−4.687
6518.37	Fe I	2.831	−2.440
6592.91	Fe I	2.727	−1.473
6593.87	Fe I	2.433	−2.420
6609.11	Fe I	2.559	−2.691
6677.99	Fe I	2.690	−1.420
7748.27	Fe I	2.949	−1.751
7780.56	Fe I	4.473	−0.010
4731.45	Fe II	2.891	−3.100
6516.08	Fe II	2.891	−3.310
7711.72	Fe II	3.903	−2.500

3.2 Chemical abundance determination

Chemical abundances were determined for Fe (using Fe I and Fe II), Na (Na I), O (O I), Mg (Mg I), and Al (Al I) using the EW method. EWs of absorption lines were measured using a combination of the ARES (Sousa et al. 2015, v2) and IRAF ONEDSPEC packages, while one-dimensional LTE abundances were determined using the MOOG code (Sneden 1973, 2014 June release) and model atmospheres that were interpolated from the Castelli & Kurucz (2004) grid. The line list and atomic data used for this analysis are specified in Table 3. The LTE assumption has been known for many years to be an inaccurate approximation for the abundances of many elemental species. In fact, all elements determined in this work are affected by non-LTE effects which must be accounted for if the abundances are to be reliable. Fortunately, grids of non-LTE corrections now exist for all of these elements in the parameter space occupied by our stellar sample.

Iron abundances determined from neutral absorption lines are known to be systematically lower than those determined using singly ionized lines (for which LTE is a realistic approximation; Lind et al. 2012). However, due to the large number of Fe lines in a stellar spectrum, it can prove difficult to perform a complete line-by-line non-LTE analysis using published grids. For this reason, we performed a test to gauge the magnitude of the offsets on a subset of stars and lines. For our test, we selected a representative subsample of three RGB and three AGB stars from NGC 6397, and interpolated corrections from Amarsi et al. (2016b) for five Fe I

Table 4. Summary of average non-LTE corrections for each element, with 1σ standard deviations over the stellar sample.

Species	Average non-LTE correction	
	RGB	AGB
Fe I	$+0.08 \pm 0.04$	$+0.08 \pm 0.03$
Fe II	<0.01	<0.01
O	-0.05 ± 0.01	-0.06 ± 0.01
Na	-0.06 ± 0.02	-0.06 ± 0.01
Mg	$+0.02 \pm 0.01$	$+0.02 \pm 0.01$
Al	-0.06 ± 0.03	-0.05 ± 0.05

lines[1] and two Fe II lines.[2] The results of this test are summarized in the first two rows of Table 4. We did not apply these average corrections, but compare them to our LTE Fe results in Section 4.

Non-LTE corrections were applied to all Na, O, Mg, and Al abundances line-by-line using the most recent grids. As in ML16, Na abundances were determined using the 568 nm doublet and corrected for non-LTE effects as described in Lind et al. (2011b) by using the web-based INSPECT interface,[3] and adopting the provided Δ[Na/Fe]$_{\rm nlte}$ corrections. The oxygen 777 nm triplet was measured and non-LTE corrections were determined by the interpolation of the recent Amarsi et al. (2016a) grid of corrections. For Mg, the measured EWs of the 571 nm and 769 nm lines were used for non-LTE determinations as described in Osorio & Barklem (2016), using the INSPECT interface. The average of these two values was then used to correct the 473 nm Mg line. Finally, both the 669 and 783 nm doublets were used to determine Al abundances, while non-LTE adjustments were interpolated from the new results of Nordlander & Lind (2017). Average non-LTE corrections and associated spreads are listed in Table 4.

4 ABUNDANCE RESULTS AND ANALYSIS

Final elemental abundances are presented in Table 5. Uncertainties cited in the table are based only on the line-to-line scatter of each abundance and do not consider additional sources of error. Using our estimated 1σ uncertainties of each stellar parameter ($\pm$50 K in $T_{\rm eff}$, $\pm$0.1 in log g, and $\pm$0.2 km s^{-1} in $v_{\rm t}$), an atmospheric sensitivity analysis was performed on a representative subsample and results are summarized in Table 6. Finally, in Table 7, we present a summary of all identified sources of uncertainties and adopted total abundance uncertainties.

A comparison of our results was made with that of L11, Lind et al. (2011b), and Carretta et al. (2009a, C09), with which we had a total of five and 21 RGB stars in common, respectively. The results of the detailed comparison of all stellar parameters and abundances are presented in Table 8, which shows good agreement in all stellar parameters and slight to moderate offsets in abundance results (0.03–0.18 dex) between the studies. These offsets arise from different methods in analysis.

In the cases of assumed stellar mass, atmospheric model parameters, adopted non-LTE corrections, and adopted solar abundances, we were able to quantify the effects since the previous studies published their values for these inputs. These sources of uncertainty combine to total possible offsets of up to +0.10 dex in each abundance. Other sources of uncertainty which we could not quantify (because we do not have the relevant information from the related studies), for example different line lists, EW measurements, and instrumentation differences, most likely explain the remaining offsets. We note that the scatter around these offsets is typically considered a better indication of the agreement between abundance analysis studies, and is consistent with the uncertainties quoted in this work. We find very good agreement between our study and that of L11. A curiosity here is the lack of agreement on microturbulence values with C09. While we adopted photometric $v_{\rm t}$ (and therefore had a relatively small spread in values, ranging from 1.52 to 1.71 km s^{-1}), C09 determined microturbulence spectroscopically and had a very large spread in $v_{\rm t}$ values (ranging from 0.11 to 2.73 km s^{-1} in the overlapping sample). This may explain the increased offsets and scatter between C09 and our study.

The difference between our mean LTE [Fe I/H] and [Fe II/H] abundances[4] (from Table 5) across our sample is $<\delta$Fe$> = -0.14 \pm 0.01$ ($\sigma = 0.05$). This is 0.06 dex lower than value predicted by non-LTE theory (-0.08 ± 0.05 dex, see Section 3.2 and Fig. 3). While this could indicate slight systematics in either our $T_{\rm eff}$ estimates or the non-LTE corrections, the uncertainty range of our $<\delta$Fe$>$ value overlaps with that of the non-LTE predicted δFe value, indicating broad agreement. Our Fe abundances are consistent with literature values ($<$[Fe/H]$>_{\rm L11} = -2.08 \pm 0.02$). Furthermore, the difference between the average RGB and AGB δFe values is less than 0.015 dex for NGC 6397, indicating that there are no significant offsets in δFe between the two giant branches, as has been disputed for NGC 6752 (Lapenna et al. 2016; C17). This is presented visually in Fig. 3, where the overall homogeneity of Fe abundances can be seen, especially between the AGB and RGB.

Abundances of elements other than iron are presented in Figs 4–6. NGC 6397 was shown by L11 to have both Na–O and Mg–Al anticorrelations, which we find on both the RGB and AGB, along with a Na–Al correlation (Fig. 6). The abundance distributions of the two giant branches in NGC 6397 are remarkably similar – we find that $\mathscr{R}_{\rm RGB} \simeq \mathscr{R}_{\rm AGB} \simeq 60$ per cent (compared with $\mathscr{R}_{\rm RGB} \simeq 75$ per cent in L11), indicating no SP2 AGB deficit, i.e. $\mathscr{F} \simeq 0$ per cent. This is in agreement with current stellar evolutionary theory, which predicts that there should be no AGB-manqué stars in NGC 6397, due to an HB that only extends to $T_{\rm eff} \simeq 10\,500$ K (Greggio & Renzini 1990; Dorman et al. 1993; Lovisi et al. 2012).

Finally, in Fig. 7, we present Gaussian kernel density estimations (KDEs) of our AGB and RGB samples. We also plot KDEs of the RGB samples from L11 and C09 for a comparison. Constant corrections of -0.03 and -0.17 dex, respectively, were applied to the data of these studies based on the systematic [Na/H] offsets determined (Table 8). Fig. 7 shows excellent agreement between the [Na/H] abundances of our current RGB and AGB samples, as well as between our RGB results and the RGB results of L11 and C09.

5 DISCUSSION AND CONCLUSIONS

The primary goal of this study was to determine the proportion of SP2 stars in NGC 6397 that evolve through to the AGB phase. Since the work of Campbell et al. (2013), the nature of AGB stars in GCs has been debated in the literature, with eight high-resolution spectroscopic studies (García-Hernández et al. 2015; Johnson et al. 2015; Lapenna et al. 2015, 2016; ML16; Wang et al. 2016, 2017; Marino

[1] 4788.8, 4839.5, 5701.6, 5753.1, and 7748.3 Å.
[2] 6516.1 and 7711.7 Å.
[3] http://inspect-stars.net

[4] δFe = [Fe I/H] − [Fe II/H].

Table 5. Stellar parameters and derived chemical abundances for each star in NGC 6397. Abundance uncertainties reflect line-to-line scatter (1σ), and do not take atmospheric sensitivities into account (see Table 6, and the text for discussion). The last two rows are the cluster average abundances with error on the mean, and standard deviation to indicate observed scatter. We adopt the Asplund et al. (2009) solar abundance values. The full table is available online.

ID	Type	$T_{\rm eff}$ (K)	log g (cgs)	$v_{\rm t}$ (km s^{-1})	[Fe I/H]	[Fe II/H]	[O/H]	[Na/H]	[Mg/H]	[Al/H]
56897	AGB	4978	1.80	1.64	-2.13 ± 0.06	-2.00 ± 0.02	-1.64 ± 0.01	-1.92 ± 0.01	-1.84 ± 0.04	-1.32 ± 0.03
60609	AGB	4905	1.70	1.67	-2.23 ± 0.07	-2.06 ± 0.01	-1.45 ± 0.04	-1.98 ± 0.01	-2.02 ± 0.01	-1.37 ± 0.01
70509	AGB	5017	1.88	1.61	-2.18 ± 0.06	-2.07 ± 0.04	-1.49 ± 0.04	-2.15 ± 0.01	-1.79 ± 0.05	-1.53 ± 0.04
70522	AGB	4739	1.42	1.76	-2.24 ± 0.05	-2.06 ± 0.03	-1.63 ± 0.02	-1.94 ± 0.04	-1.99 ± 0.08	-1.48 ± 0.06
73216	AGB	4968	1.80	1.64	-2.16 ± 0.05	-2.04 ± 0.00	-1.39 ± 0.06	-2.29 ± 0.04	-1.73 ± 0.05	-1.67 ± 0.03
⋮	⋮	⋮	⋮	⋮	⋮	⋮	⋮	⋮	⋮	⋮
Mean					-2.15 ± 0.01	-2.02 ± 0.00	-1.52 ± 0.02	-2.06 ± 0.02	-1.87 ± 0.01	-1.49 ± 0.02
σ					0.05	0.03	0.12	0.19	0.11	0.16

Table 6. Typical abundance uncertainties due to the (1σ) atmospheric sensitivities of a representative subsample of three RGB and two AGB stars in our NGC 6397 data set. Parameter variations (in parentheses) are the expected uncertainties in the respective parameters.

	$\Delta T_{\rm eff}$ ($\pm$50 K)	Δlog g ($\pm$0.1 dex)	$\Delta v_{\rm t}$ ($\pm$0.2 km s^{-1})	Total
[Fe I/H]	$\pm$0.06	$\mp$0.01	$\mp$0.04	$\pm$0.04
[Fe II/H]	$\mp$0.01	$\pm$0.04	$\mp$0.01	$\pm$0.04
[O/H]	$\mp$0.06	$\pm$0.04	$\pm$0.00	$\pm$0.07
[Na/H]	$\pm$0.03	$\mp$0.01	$\pm$0.00	$\pm$0.03
[Mg/H]	$\pm$0.03	$\mp$0.00	$\pm$0.00	$\pm$0.03
[Al/H]	$\pm$0.03	$\pm$0.00	$\pm$0.00	$\pm$0.03

Table 7. Summary of typical abundance uncertainties (1σ) from each source identified in the text, and the total uncertainties (added in quadrature). The first column shows the average line-to-line uncertainties of all stars, values in the second column are the total uncertainties from atmospheric sensitivities (Table 6), and the third column represents the typical uncertainties quoted in each non-LTE source (see Section 3.2 for citations). Note that individual Fe abundances were not corrected for non-LTE (see the text for details).

Species	Line-to-line	Atmospheric	non-LTE	Total
Fe I	$\pm$0.07	$\pm$0.04	–	$\pm$0.08
Fe II	$\pm$0.03	$\pm$0.04	–	$\pm$0.05
O	$\pm$0.03	$\pm$0.07	$\pm$0.05	$\pm$0.09
Na	$\pm$0.04	$\pm$0.03	$\pm$0.04	$\pm$0.06
Mg	$\pm$0.04	$\pm$0.03	$\pm$0.03	$\pm$0.06
Al	$\pm$0.04	$\pm$0.03	$\pm$0.06	$\pm$0.08

Table 8. The average differences in parameters and abundances between this work and that of L11 and Carretta et al. (2009a, C09). Uncertainties are standard deviations, and indicate the scatter around the offsets. While significant offsets exist between our work and the works of L11 and C09, the scatter around the offsets are consistent with the uncertainties quoted in this work (see the text for discussion).

Parameter	This study – L11	This study – C09
$\Delta T_{\rm eff}$	-4.3 ± 20.9	19.5 ± 29.9
Δlog g	0.08 ± 0.01	0.07 ± 0.02
$\Delta v_{\rm t}$	0.04 ± 0.03	0.21 ± 0.64
Δ[Fe I/H]	-0.08 ± 0.03	-0.13 ± 0.05
Δ[Fe II/H]	0.12 ± 0.03	0.05 ± 0.05
Δ[O/H]	0.06 ± 0.08	0.18 ± 0.14
Δ[Na/H]	-0.03 ± 0.06	-0.17 ± 0.14
Δ[Mg/H]	-0.09 ± 0.03	–
Δ[Al/H]	0.17 ± 0.12	–

et al. 2017) and five photometric studies (Monelli et al. 2013; Milone et al. 2015a,b; Gruyters et al. 2017; Lardo et al. 2017) targeting the AGB directly, along with five theoretical studies seeking to explain the anomalous observations (Charbonnel et al. 2013, 2014; Cassisi et al. 2014; Charbonnel & Chantereau 2016).

Since only HB stars with effective temperatures above ~15 000 K are predicted to evolve directly to the white dwarf phase, the AGBs of clusters that lack an extended blue HB are expected to contain distributions in Na, O, Mg, and Al abundances that are statistically indistinguishable from those of the RGB – all cluster stars should evolve through both giant branches (i.e. $\mathscr{F} \simeq 0$ per cent). Only in clusters with extended blue HBs should the distribution be different, and only with the ~30 per cent most extreme (Na-rich/O-poor/Al-rich) AGB stars missing (i.e. $\mathscr{F} \simeq 30$ per cent Dorman et al. 1993; Cassisi et al. 2014).

Despite a rapidly expanding literature sample of GC AGB studies, the picture is still far from clear. To date, 11 GCs have had their AGB systematically probed with high-resolution spectrographs,[5] with mixed results in $\mathscr{F}$ values (see ML16, Table 4). However, only three clusters have been reported to have $\mathscr{F} \simeq 100$ per cent: NGC 6752 (Campbell et al. 2013, C17), M62 (Lapenna et al. 2015), and M4 (ML16). Of these, only M62 has not been disputed by subsequent studies, but we note that this GC has not yet been studied a second time.

Lapenna et al. (2016) reported that the Fe I abundances of AGB stars in NGC 6752 are lower than predicted by standard non-LTE theory. If extrapolated to Na abundance (i.e. if Na is assumed to follow this trend), the AGB [Na I/Fe I] abundance distribution moves to be in line with stellar theory ($\mathscr{F} \simeq 30$ per cent, as expected in GCs with an extended blue HB), contradicting the conclusions of Campbell et al. (2013), who claimed $\mathscr{F} \simeq 100$ per cent. However, in a detailed re-analysis of their data, C17 reported that there was no iron abundance discrepancy in NGC 6752 when more reliable $T_{\rm eff}$ scales were used, therefore concluding that the original Na results of Campbell et al. (2013) are reliable. Furthermore, for NGC 6397, we have found no significant δFe offset between the AGB and

[5] NGC 2808, NGC 6397, NGC 6752, 47 Tucanae, M2, M3, M4, M5, M13, M55, and M62.

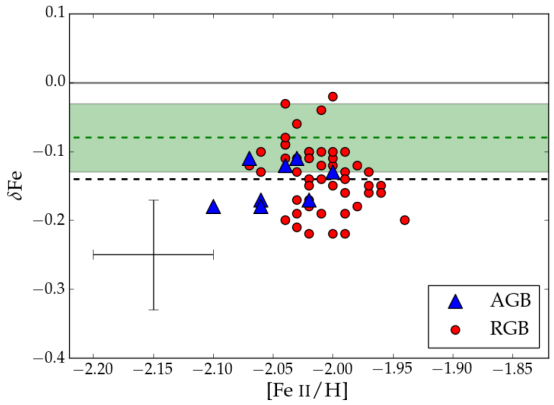

Figure 3. LTE Fe abundances for our NGC 6397 sample. Here, δFe ([Fe I/H]–[Fe II/H]) is plotted against [Fe II/H] abundance to highlight departures from LTE in Fe I, and the similarity between the Fe abundances of the AGB and RGB. The error bars indicate typical 1σ total uncertainties on individual abundances (see Table 7), while the black dashed line represents the sample average δFe value of -0.14 dex. The green dashed line represents the expected δFe value (-0.08 dex) from our non-LTE test (see Section 3.2) and the shaded region indicates the non-LTE uncertainties quoted in Amarsi et al. (2016b, ±0.05 dex).

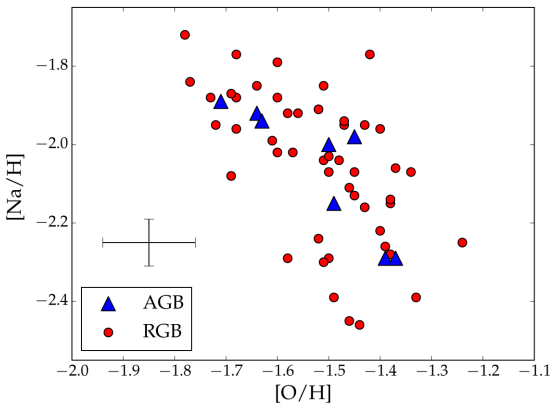

Figure 4. Na and O abundances for our NGC 6397 sample. The error bars indicate typical 1σ total uncertainties on individual abundances (see Table 7).

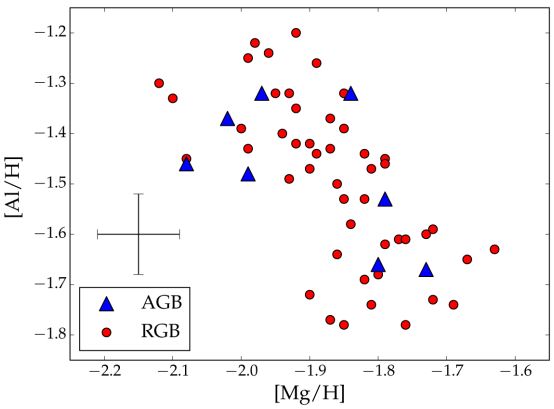

Figure 5. Same as Fig. 4, but for Mg and Al.

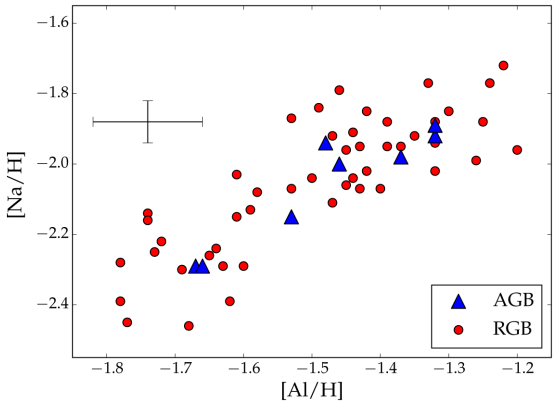

Figure 6. Same as Fig. 4, but for Na and Al.

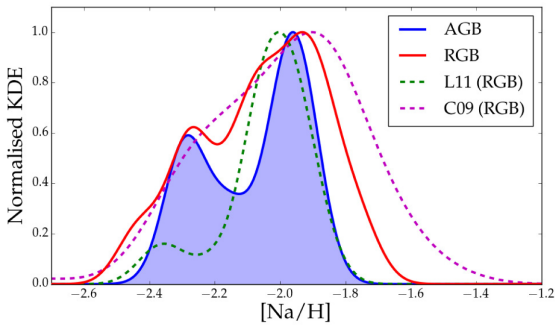

Figure 7. Gaussian KDEs of our NGC 6397 [Na/H] abundances, along with those of L11 and Carretta et al. (2009a, C09), with systematic offsets removed (see the text for details). A smoothing bandwidth of 0.06 dex (total Na uncertainty, see Table 7) was applied to each of our RGB and AGB data sets, while for C09 we used a bandwidth of 0.11 dex, matching their total error calculations (see C09, Appendix A). L11 did not quote total abundance uncertainties, however their average measurement uncertainty in Na was the same as in our sample (0.04 dex), therefore we applied an identical bandwidth of 0.06 dex. The discrepancy between the relative heights of the two peaks in the L11 sample, compared to those of the other samples, may be due to the low number of stars observed in L11 (21 RGB stars).

RGB, and that the Fe abundances are internally homogeneous (at the level of our uncertainties). This allows [X/H] abundances to be used for the elemental distribution analyses of the giant branches, because using [X/Fe] would introduce additional scatter (through measurement uncertainties), but no new information.

The abundances of NGC 6397 (Figs 4–7) contain no evidence of an SP2 AGB deficit, with the relative distributions of the RGB and AGB being identical in all abundance planes ($\mathscr{F} \simeq 0$ per cent).

It is interesting to compare this result with that of M4 by ML16, since the methods and tools we have used are almost identical. The only difference between the NGC 6397 analysis performed in this study and that of ML16 is the method of determining atmospheric parameters. In ML16, $T_{\rm eff}$, log g, and $v_{\rm t}$ values were determined spectroscopically by requiring excitation and ionization balance (as per Sousa 2014), whereas for NGC 6397 these parameters were estimated through photometric relations. As shown in C17, Na I abundances are quite robust, that is they are not as sensitive to systematic shifts in $T_{\rm eff}$ as Fe I abundances. We have also shown that our Fe results are consistent with non-LTE theory, and show homogeneous abundances in both ionization states, indicating that our $T_{\rm eff}$ scale is accurate. For these reasons, we consider that the different method

of parameter determination between our two studies should have little consequence on the reliability of our [Na/H] abundances.

Thus, our NGC 6397 result further strengthens the conclusions of ML16 whose analysis was almost identical, but whose results are in contradistinction. We therefore suggest that our original M4 conclusions ($\mathscr{F} \simeq 100$, but with some uncertainty) are sound, and that our NGC 6397 results show, by providing a control sample, that our method of analysis does not artificially shift AGB abundances towards SP1-like distributions.

As stated in ML16, our M4 result ($\mathscr{F} \simeq 100$) is in clear contradiction with stellar theory – we can think of no reason why SP2 stars in M4 should avoid the AGB phase, since the maximum $T_{\rm eff}$ of its HB is ∼9000 K (Marino et al. 2011). This is especially true in light of our result for NGC 6397, which has a bluer HB than M4, but $\mathscr{F} \simeq 0$ per cent. In the search for a possible explanation of our results, and those of Campbell et al. (2013), C17 (NGC 6752), and Lapenna et al. (2015, M62), we consider three possible causes of the low-Na signature of AGB stars in M4, NGC 6752, and M62.

(i) The low-Na signature is intrinsic – HB stars are becoming AGB-manqué stars at a much lower HB $T_{\rm eff}$ than predicted. This is the most commonly cited explanation in the literature.

(ii) The atmospheric models of some AGB stars are incorrectly determined, but only in particular sections of the GC AGB parameter space. This would result in incorrectly predicted absorption line profiles, and represent a significant 'blind spot' in the standard spectroscopic method.

(iii) All Na-rich stars in these three GCs are undergoing an unknown burning or mixing process, between the HB and AGB, that acts to deplete Na in the envelope and leaves only a low-Na signature by the early AGB phase.

Investigating these hypotheses is beyond the scope of this work. However, we note that (iii) is almost certainly impossible since there is no known mechanism that can destroy Na, while simultaneously creating O, in the interior conditions found in these stars.

More generally, we note that, of the GCs which have been analysed for SP2 AGB deficits, not a single deficit (or lack thereof) claim has been confirmed by a different working group, or with independently selected targets. This suggests that the methods that are used require detailed investigation and checking, such as performed in C17. This is especially pertinent for M4, for which the three existing studies all give different values of $\mathscr{F}$. We will aim to resolve this issue in a forthcoming study. Finally, we suggest another potential next step in investigating this problem could be a controlled spectroscopic study of an 'HB second parameter' pair or trio of clusters with similar metallicity and age, but a different HB-morphology (such as NGC 288, NGC 362, and NGC 1851), in an attempt to disentangle the effect of global GC parameters on apparent AGB deficits.

ACKNOWLEDGEMENTS

Based in part on data acquired through the AAO, via programme 15A/21 (PI Campbell). Part of this work was supported by the DAAD (PPP project 57219117) with funds from the German Federal Ministry of Education and Research (BMBF). BTM acknowledges the financial support of his Australian Postgraduate Award scholarship. SWC acknowledges federal funding from the Australian Research Council though the Future Fellowship grant entitled 'Where are the Convective Boundaries in Stars?' (FT160100046). VD acknowledges support from the AAO distinguished visitor programme 2016. LC gratefully acknowledges support from the Australian Research Council (grants DP150100250, FT160100402). We thank Anish Amarsi and Thomas Nordlander for providing non-LTE corrections, and Michael Brown, Alexander Heger, and the referee for useful conversations, comments, and advice.

REFERENCES

AAO Software Team, 2015, Astrophysics Source Code Library, record ascl:1505.015
Alonso A., Arribas S., Martínez-Roger C., 1999, A&AS, 140, 261
Amarsi A. M., Asplund M., Collet R., Leenaarts J., 2016a, MNRAS, 455, 3735
Amarsi A. M., Lind K., Asplund M., Barklem P. S., Collet R., 2016b, MNRAS, 463, 1518
Asplund M., Grevesse N., Sauval A. J., Scott P., 2009, ARA&A, 47, 481
Bergemann M., Lind K., Collet R., Magic Z., Asplund M., 2012, MNRAS, 427, 27
Campbell S. W., Yong D., Wylie-de B. E. C., Stancliffe R. J., Lattanzio J. C., Angelou G. C., Grundahl F., Sneden C., 2010, Mem. Soc. Astron. Ital., 81, 1004
Campbell S. W. et al., 2013, Nature, 498, 198
Campbell S. W., MacLean B. T., D'Orazi V., Casagrande L., de Silva G. M., Yong D., Cottrell P. L., Lattanzio J. C., 2017, A&A, 605, A98(C17)
Cannon R. D., Croke B. F. W., Bell R. A., Hesser J. E., Stathakis R. A., 1998, MNRAS, 298, 601
Carretta E. et al., 2009a, A&A, 505, 117
Carretta E., Bragaglia A., Gratton R., D'Orazi V., Lucatello S., 2009b, A&A, 508, 695
Carretta E., Bragaglia A., Gratton R. G., Recio-Blanco A., Lucatello S., D'Orazi V., Cassisi S., 2010, A&A, 516, A55
Casagrande L., Ramírez I., Meléndez J., Bessell M., Asplund M., 2010, A&A, 512, A54
Casagrande L. et al., 2014, MNRAS, 439, 2060
Cassisi S., Salaris M., Pietrinferni A., Vink J. S., Monelli M., 2014, A&A, 571, A81
Castelli F., Kurucz R. L., 2004, preprint (astro-ph/0405087)
Charbonnel C., Chantereau W., 2016, A&A, 586, A21
Charbonnel C., Chantereau W., Decressin T., Meynet G., Schaerer D., 2013, A&A, 557, L17
Charbonnel C., Chantereau W., Krause M., Primas F., Wang Y., 2014, A&A, 569, L6
Cottrell P. L., Da Costa G. S., 1981, ApJ, 245, L79
De Silva G. M., Gibson B. K., Lattanzio J., Asplund M., 2009, A&A, 500, L25
De Silva G. M. et al., 2015, MNRAS, 449, 2604
Dorman B., Rood R. T., O'Connell R. W., 1993, ApJ, 419, 596
García-Hernández D. A., Mészáros S., Monelli M., Cassisi S., Stetson P. B., Zamora O., Shetrone M., Lucatello S., 2015, ApJ, 815, L4
González Hernández J. I., Bonifacio P., 2009, A&A, 497, 497
Gratton R. G., Carretta E., Castelli F., 1996, A&A, 314, 191
Gratton R. G. et al., 2001, A&A, 369, 87
Gratton R. G., Bragaglia A., Carretta E., Clementini G., Desidera S., Grundahl F., Lucatello S., 2003, A&A, 408, 529
Gratton R., Sneden C., Carretta E., 2004, ARA&A, 42, 385
Gratton R. G., D'Orazi V., Bragaglia A., Carretta E., Lucatello S., 2010, A&A, 522, A77
Gratton R. G., Carretta E., Bragaglia A., 2012, A&AR, 20, 50
Greggio L., Renzini A., 1990, ApJ, 364, 35
Gruyters P., Casagrande L., Milone A. P., Hodgkin S. T., Serenelli A., Feltzing S., 2017, A&A, 603, A37
Harris W. E., 1996, AJ, 112, 1487
Johnson C. I. et al., 2015, AJ, 149, 71
Lapenna E., Mucciarelli A., Lanzoni B., Ferraro F. R., Dalessandro E., Origlia L., Massari D., 2014, ApJ, 797, 124
Lapenna E., Mucciarelli A., Ferraro F. R., Origlia L., Lanzoni B., Massari D., Dalessandro E., 2015, ApJ, 813, 97

Lapenna E. et al., 2016, ApJ, 826, L1
Lardo C., Salaris M., Savino A., Donati P., Stetson P. B., Cassisi S., 2017, MNRAS, 466, 3507
Lind K., Primas F., Charbonnel C., Grundahl F., Asplund M., 2009, A&A, 503, 545
Lind K., Charbonnel C., Decressin T., Primas F., Grundahl F., Asplund M., 2011a, A&A, 527, A148(L11)
Lind K., Asplund M., Barklem P. S., Belyaev A. K., 2011b, A&A, 528, A103
Lind K., Bergemann M., Asplund M., 2012, MNRAS, 427, 50
Lovisi L., Mucciarelli A., Lanzoni B., Ferraro F. R., Gratton R., Dalessandro E., Contreras Ramos R., 2012, ApJ, 754, 91
MacLean B. T., De Silva G. M., Lattanzio J., 2015, MNRAS, 446, 3556
MacLean B. T., Campbell S. W., De Silva G. M., Lattanzio J., D'Orazi V., Simpson J. D., Momany Y., 2016, MNRAS, 460, L69(ML16)
Marino A. F., Villanova S., Milone A. P., Piotto G., Lind K., Geisler D., Stetson P. B., 2011, ApJ, 730, L16
Marino A. F. et al., 2017, ApJ, 843, 66
Miglio A. et al., 2016, MNRAS, 461, 760
Milone A. P. et al., 2008, ApJ, 673, 241
Milone A. P., Marino A. F., Piotto G., Bedin L. R., Anderson J., Aparicio A., Cassisi S., Rich R. M., 2012, ApJ, 745, 27
Milone A. P. et al., 2014, MNRAS, 439, 1588
Milone A. P. et al., 2015a, MNRAS, 447, 927
Milone A. P. et al., 2015b, ApJ, 808, 51
Momany Y., Cassisi S., Piotto G., Bedin L. R., Ortolani S., Castelli F., Recio-Blanco A., 2003, A&A, 407, 303
Monelli M. et al., 2013, MNRAS, 431, 2126
Nordlander T., Lind K., 2017, A&A, 607, A75
Norris J., 1981, ApJ, 248, 177
Norris J., Cottrell P. L., Freeman K. C., Da Costa G. S., 1981, ApJ, 244, 205
Osorio Y., Barklem P. S., 2016, A&A, 586, A120
Ramírez I., Meléndez J., 2005, ApJ, 626, 465
Schiavon R. P. et al., 2017, MNRAS, 465, 501
Sheinis A. et al., 2015, J. Astron. Telesc. Instrum. Syst., 1, 035002
Skrutskie M. F. et al., 2006, AJ, 131, 1163
Sneden C. A., 1973, PhD thesis, Univ. Texas
Sousa S. G., 2014, in Niemczura E., Smalley B., Pych W., eds, Determination of Atmospheric Parameters of B-, A-, F- and G-Type Stars. Springer, Berlin, p. 297
Sousa S. G., Santos N. C., Adibekyan V., Delgado-Mena E., Israelian G., 2015, A&A, 577, A67
Tody D., 1986, in Crawford D. L., ed., Proc. SPIE Conf. Ser. Vol. 627, Instrumentation in Astronomy VI. SPIE, Bellingham, p. 733
Wang Y., Primas F., Charbonnel C., Van der Swaelmen M., Bono G., Chantereau W., Zhao G., 2016, A&A, 592, A66
Wang Y., Primas F., Charbonnel C., Van der Swaelmen M., Bono G., Chantereau W., Zhao G., 2017, A&A, 607, A135

SUPPORTING INFORMATION

Supplementary data are available at *MNRAS* online.

Table 1. NGC 6397 target details including data from Momany et al. (2003, *UBVI* photometry and target IDs) and 2MASS (Skrutskie et al. 2006, *JHK* photometry – gaps in data represent targets with low-quality flags), radial velocities (km s^{-1}), and Lind et al. (2011a, L11).

Table 5. Stellar parameters and derived chemical abundances for each star in NGC 6397. Abundance uncertainties reflect line-to-line scatter (1σ), and do not take atmospheric sensitivities into account (see Table 6, and the text for discussion). The last two rows are the cluster average abundances with error on the mean, and standard deviation to indicate observed scatter.

Please note: Oxford University Press is not responsible for the content or functionality of any supporting materials supplied by the authors. Any queries (other than missing material) should be directed to the corresponding author for the article.

This paper has been typeset from a TEX/LATEX file prepared by the author.